Dynamics of thermochemical plumes: 2. Complexity of plume structures and its implications for mapping mantle plumes

Shu-Chuan Lin

Department of Geological Sciences, University of Michigan, 2534 C. C. Little Building, 1100 North University, Ann Arbor, Michigan 48109, USA

Now at Department of Geosciences, National Taiwan University, 1, Section 4, Roosevelt Road, Taipei 106, Taiwan (skylin0@ntu.edu.tw)

Peter E. van Keken

Department of Geological Sciences, University of Michigan, 2534 C. C. Little Building, 1100 North University, Ann Arbor, Michigan 48109, USA (keken@umich.edu)

[1] The mantle plume hypothesis provides explanations for several major observations of surface volcanism. The dynamics of plumes with purely thermal origin has been well established, but our understanding of the role of compositional variations in the Earth's mantle on plume formation is still incomplete. In this study we explore the structures of plumes originating from a thermochemical boundary layer at the base of the mantle in an attempt to complement fluid dynamical studies of purely thermal plumes. Our numerical experiments reveal diverse characteristics of thermochemical plumes that frequently deviate from the classic features of plumes. In addition, owing to the interplay between the thermal and compositional buoyancy forces, the morphology, temperature, and flow fields in both the plume head and plume conduit are strongly time-dependent. The entrainment of the dense layer and secondary instabilities developed in the boundary layer contribute to lateral heterogeneities and enhance stirring processes in the plume head. Our models show that substantial topography of the compositional layer can develop simultaneously with the plumes. In addition, plumes may be present in the lower mantle for more than 70 million years. These features may contribute to the large low seismic velocity provinces beneath the south central Pacific, the southern Atlantic Ocean, and Africa. Our model results support the idea that the dynamics of mantle plumes is much more complicated than conventional thinking based on studies of purely thermal plumes. The widely used criteria for mapping mantle plumes, such as a vertically continuous low seismic velocity signature and strong surface topography swell, may not be universally applicable. We propose that the intrinsic density contrast of the distinct composition may reduce the associated topography of some large igneous provinces such as Ontong Java.

1. Introduction

[2] Several major observations of surface volcanism are not explained by the paradigm of plate tectonics. These features include intraplate volcanism commonly with a linear age progression (e.g., Hawaii), large igneous provinces (e.g., Deccan Traps, Ontong Java Plateau), sections of spreading centers with over-thickened crust (e.g., Iceland), excess magmatism in rift zones (e.g., East Africa) and the distinctive geochemistry between the oceanic island basalts (OIB) and mid-oceanic ridge basalts (MORB). The hypothesis of mantle plumes has been a widely accepted model to account for these features by a single mechanism [e.g., *Morgan*, 1971; *Richards et al.*, 1989; *Sleep*, 1990; *Davies*, 1999; *Condie*, 2001]. Plumes are likely to be generated from the base of the mantle which contains a significant thermal boundary layer with a temperature increase of ∼1000 K or more at the base of the lower mantle [e.g., *Jeanloz and Morris*, 1986; *Boehler*, 2000; *Steinle-Neumann et al.*, 2001]. The dynamics of the thermal plumes have been well established by laboratory and numerical experiments [e.g., *Whitehead and Luther*, 1975; *Olson and Singer*, 1985; *Griffiths and Campbell*, 1990; *van Keken*, 1997; *Kellogg and King*, 1997] and has led to the hypothesis that a voluminous plume head followed by a narrow feeding conduit explains both the formation of the large igneous provinces and the age progression of the subsequent hot spot tracks.

[3] Notwithstanding some progress in recent years [e.g., *Wolfe et al.*, 1997; *Shen et al.*, 1998; *Montelli et al.*, 2004], direct detection of mantle plumes by seismic methods has been proven difficult. This is partly expected due to the low velocity and small scale nature of mantle plumes, combined with sparse seismometer coverage near oceanic islands. A number of geodynamical and seismological studies provide quantitative explanations for the difficulties in mapping mantle plumes [e.g., *Tackley*, 2002; *Goes et al.*, 2004; *Farnetani and Samuel*, 2005].

[4] Several alternative hypotheses exist for the formation of aforementioned magmatism [e.g., *Anderson*, 1998, 2004; *Foulger and Natland*, 2003; *Ingle and Coffin*, 2004] but it is difficult to understand how the heat for long-lived volcanism can be supplied in area that away from active rifting or how the excess magma can be formed in spreading centers or rift zones without substantial and long-lived vertical advection of hot material (i.e., a mantle plume).

[5] A number of criteria can be used to characterize whether certain geographic areas fit the mantle plume theory. These include (1) linear age progression of intraplate volcanism, (2) the presence of a flood basalt at the origin of the volcanic track, (3) vertically continuous low seismic velocity signatures associated with the proposed hot spot, (4) elevated topography associated intraplate volcanism, (5) high helium ratio signature and distinct geochemistry in the volcanism [e.g., *Ritsema and Allen*, 2003; *Courtillot et al.*, 2003]. Recent studies show that only less than ten previously proposed hot spots may fulfill these criteria [e.g., *Ritsema and Allen*, 2003; *Courtillot et al.*, 2003]. However, the large igneous provinces at the origin of the hot spot tracks in some cases may have entered the deep interior of the Earth's mantle by subduction (e.g., Hawaii). The age progression pattern may not be generated because the magmatism may not align with the path of the plume center due to topography of base of the lithosphere that can modulate the melt generation [e.g., *Ebinger and Sleep*, 1998; *Lin et al.*, 2005].

[6] Thermal plumes rising from the thermal boundary layer at the core-mantle boundary will be influenced by the physical and chemical properties of this boundary layer. There is increasing consensus of a compositionally distinct layer in the lower mantle [e.g., *Loper and Lay*, 1995; *van der Hilst*, 2004; *Lay and Garnero*, 2004; *Rost et al.*, 2005]. The origin of the compositional layer remains controversial and several mechanisms, such as the accumulation of the recycled oceanic crust, partial melting of mantle, chemical reaction between core and mantle, or the early differentiation of Earth, have been proposed to contribute to its formation [e.g., *Christensen and Hofmann*, 1994; *Manga and Jeanloz*, 1996; *William and Garnero*, 1996; *Kellogg et al.*, 1999; *Rost et al.*, 2005]. The structure and behavior of mantle plumes is expected to be strongly modified in the presence of such a dense layer in the lowermost mantle. Previous studies reveal that superswells and hot spots can be formed simultaneously in a thermochemical convection system [e.g., *Davaille*, 1999; *Farnetani and Samuel*, 2005]. *Farnetani and Samuel* [2005] show that a headless plume of deep origin can produce volcanism with distinct age progression.

[7] In order to better understand the role of the proposed dense layer at the base of the mantle on plume dynamics we have developed plume models in an axisymmetric spherical shell in which we systematically vary the thickness and density contrast of the dense layer. In a companion paper [*Lin*
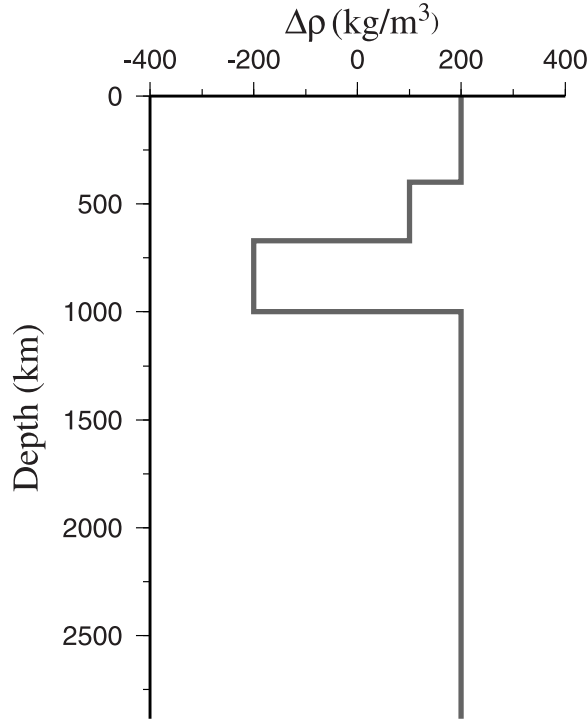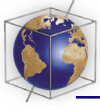
Figure 1. Reference depth profile for excess density of eclogite [*Lin and van Keken*, 2005].

and van Keken, 2006] we have detailed the methodology and provided an overview of the general characteristics governing the formation of thermochemical plumes and the entrainment of the dense layer. For the isoviscous case we have found that this provide good agreement with previous work, as is shown in the Appendix. In this paper we particularly focus on the morphology of thermochemical plumes and the consequences of the dense layer on the detailed plume structure and evolution in models with strongly temperature-dependent rheology.

2. Model Formulation

[8] We will build on the work of two previous studies [*Lin and van Keken*, 2005, 2006] in which we systematically investigate plume evolution from a thermal boundary layer in the presence of a dense chemical layer. We assume this to be recycled oceanic crust and refer to this as "eclogite" for simplicity in the rest of the paper. Seismic tomographic models indicate significant mass exchange between the upper mantle and lower mantle by coherent, anomalous high-velocity structures from upper mantle to the lower mantle which correspond to regions of paleosubduction [e.g., *Grand et al.*, 1997; *van der Hilst et al.*, 1997; *Gu et al.*, 2001; *Tan*

et al., 2002]. The subducted oceanic crust transforms into eclogite at about 70 km depth and subsequently the high-pressure mineral assemblage at greater depths. The density of subducted oceanic crust is estimated to be 2%–4% denser than the surrounding mantle except for a density inversion in the mid-mantle [e.g., *Christensen and Hofmann*, 1994; *van Keken et al.*, 1996; *Ono et al.*, 2001]. In our modeling we assume that the layer with distinct composition is a variable mixture between eclogite and the surrounding mantle material. The reference excess density of the eclogite is 200 kg/m^3 throughout the mantle, except for a density inversion of -200 kg/m^3 at 670–1000 km depth and excess density of 100 kg/m^3 at 400–670 km depth (Figure 1) [e.g., *Christensen and Hofmann*, 1994; *van Keken et al.*, 1996; *Ono et al.*, 2001].

[9] The nondimensional equations for the conservation of mass, momentum and energy and the advection equation of the compositional field in an incompressible fluid at infinite Prandtl number in an axisymmetric spherical shell are solved numerically by a code based on finite element package Sepran [*Cuvelier et al.*, 1986; *van Keken and Ballentine*, 1999; *Lin and van Keken*, 2006]. The dense layer is characterized by its thickness d (10–200 km) and density contrast $\Delta\rho$(0–400 kg/m^3 in the lowermost mantle). In our models we assume a Newtonian fluid and the viscosity is defined by $\eta = \eta_0 \exp(-bT)$ where $b = \log(10^3)$, corresponding to a maximum viscosity contrast $\Delta\eta$ of three orders of magnitude. The thermal boundary Rayleigh number is $Ra = 2.1 \times 10^6$ [*Lin and van Keken*, 2006], which is based on a reference mantle viscosity of 10^{22} Pa s, a thickness of the model domain (H) of 2885 km, a thermal diffusivity κ of 10^{-6} m^2/s, an expansivity α of 3×10^{-5} 1/K, and reference density ρ of 4000 kg/m^3 and a temperature contrast ΔT of 750 K. The initial thermal boundary layer (TBL) thickness is assumed constant at 130 km and the maximum density variation due to thermal expansion of -90 kg/m^3. The temperature contrast across the TBL is at the lower end of reasonable estimates ($\sim$500–2000 K). Increasing the temperature contrast to the high end of the estimates will change the effective Rayleigh number by a factor of 2.5, which is well within the uncertainty of the density excess and lower mantle viscosity. We will specify the dimensional values for parameters and provide the corresponding buoyancy number to allow comparison between our calculations and the published models. The buoyancy number is given by $B = \Delta\rho/\rho\alpha\Delta T$, where $\Delta\rho$ is the intrinsic density difference between the compositionally

Table 1. Model Parameters

	Model													
	I	II	III	IV	V	VI	VII	VIII	VIIII	X	XI	XII	XIII	XIV
$\Delta\rho$, kg/m³	25	40	50	55	15	50	50	65	60	60	75	75	40	40
d, km	25	100	70	100	200	50	25	100	150	175	125	80	150	125
Category	I	I	I	I	I	I	I	II	II	II	II	II	III	III
Regime	II	II	III	III	II	III	III	III	III	III	III	III	III	III

distinct material in the lowermost mantle and the overlying mantle. The corresponding compositional Rayleigh number follows as *RaB*.

3. Results

[10] Plumes originating from the thermochemical boundary at the base of the mantle were categorized to fall into two end-member regime (regimes I and II) and an intermediate regime (regime III) in previous studies [*Lin and van Keken*, 2005, 2006]. To summarize, the first end-member regime is characterized by low temperature plumes with a negligible amount of entrainment. The second end-member regime features high temperature plumes with substantial amount of entrainment. Complicated intermediate behavior is observed in regime III. In this paper, we divide our variable viscosity models into three categories based on plume morphology. Most of the models presented here are in regime III. Table 1 summarizes the model parameters of the initial thickness and intrinsic density contrast of the compositional layer for models in Figures 2–11. All these models are models with strongly temperature-dependent viscosity ($\Delta\eta$ = 1000). The models with moderate viscosity contrast can be divided into the same categories in general, except that the flow pattern and temperature field are less complicated. For clarity we show the mirror image of the plume and indicate the dimensional time of the snapshots for the plume evolution. We also supply animations to better display the development of the intricate morphology in these strongly time-dependent cases.

3.1. Category I: Voluminous Head−Narrow Tail Structure

[11] The first category of plumes occurs when the thickness or density is not sufficient to strongly modify the formation of the thermal plume. The overall plume morphology is similar to that of plumes with purely thermal origin when the thickness of the dense layer is ∼≤80 km, or the intrinsic density contrast is ∼≤40 kg/m³ and the thickness

of the compositional layer is ≥100 km. The radius of the plume head is significantly larger than that of plume tail and the TBL around the plume tail is often drained by the formation of plume. Figure 2a and Animation 1 show an example in which the development of the plume is similar to that of thermal plumes ($\Delta\rho$ = 25 kg/m³, B = 0.28, d = 25 km), except that the development of the plume is initially slightly delayed. This leads to higher temperature in the plume head and conduit and a slightly wider radius of the plume conduit. The entrainment of the compositional layer occurs at the time of plume head formation. The dense material in the plume head induces small-scale circulation and subsequently generates lateral heterogeneity. Dense material in the plume head significantly distorts the morphology of the plume head when the compositional buoyancy force is larger (e.g., Figure 2b and Animation 2: $\Delta\rho$ = 40 kg/m³, B = 0.44, d = 100 km). Frequent pulsations and complicated flow in plume can develop due to interplay between the compositional and thermal buoyancy forces (e.g., Figure 3a and Animation 3: $\Delta\rho$ = 50 kg/m³, B = 0.56, d = 70 km and Figure 3b and Animation 4: $\Delta\rho$ = 55 kg/m³, B = 0.61, d = 100 km) [see also *Lin and van Keken*, 2005]. Replenishment of the plume by the secondary instabilities stirs the plume head frequently and may cause significant lateral heterogeneity in the plume head if intrinsic heterogeneity is present in the compositional layer. When the thickness of the compositional layer is larger and the intrinsic density contrast is smaller, the compositional layer is dragged up both within and outside the thermal plume (e.g., Figure 4 and Animation 5: $\Delta\rho$ = 15 kg/m³, B = 0.17, d = 200 km).

[12] When the thickness of the compositional layer is ∼≤50 km and the intrinsic density is ≥50 kg/m³, the dense material is entrained only from the hot portions of the TBL where temperature is high enough to provide a net positive buoyancy. It forms a high-temperature plume center which is surrounded by material with lower temperature (e.g., Figure 5a and Animation 6: $\Delta\rho$ = 50 kg/m³, B = 0.56, d = 50 km). Secondary instabilities develop at

(a) Model I   ($\Delta\eta = 1000$, $\Delta\rho = 25$ kg/m^3, d = 25 km)

(b) Model II   ($\Delta\eta = 1000$, $\Delta\rho = 40$ kg/m^3, d = 100 km)
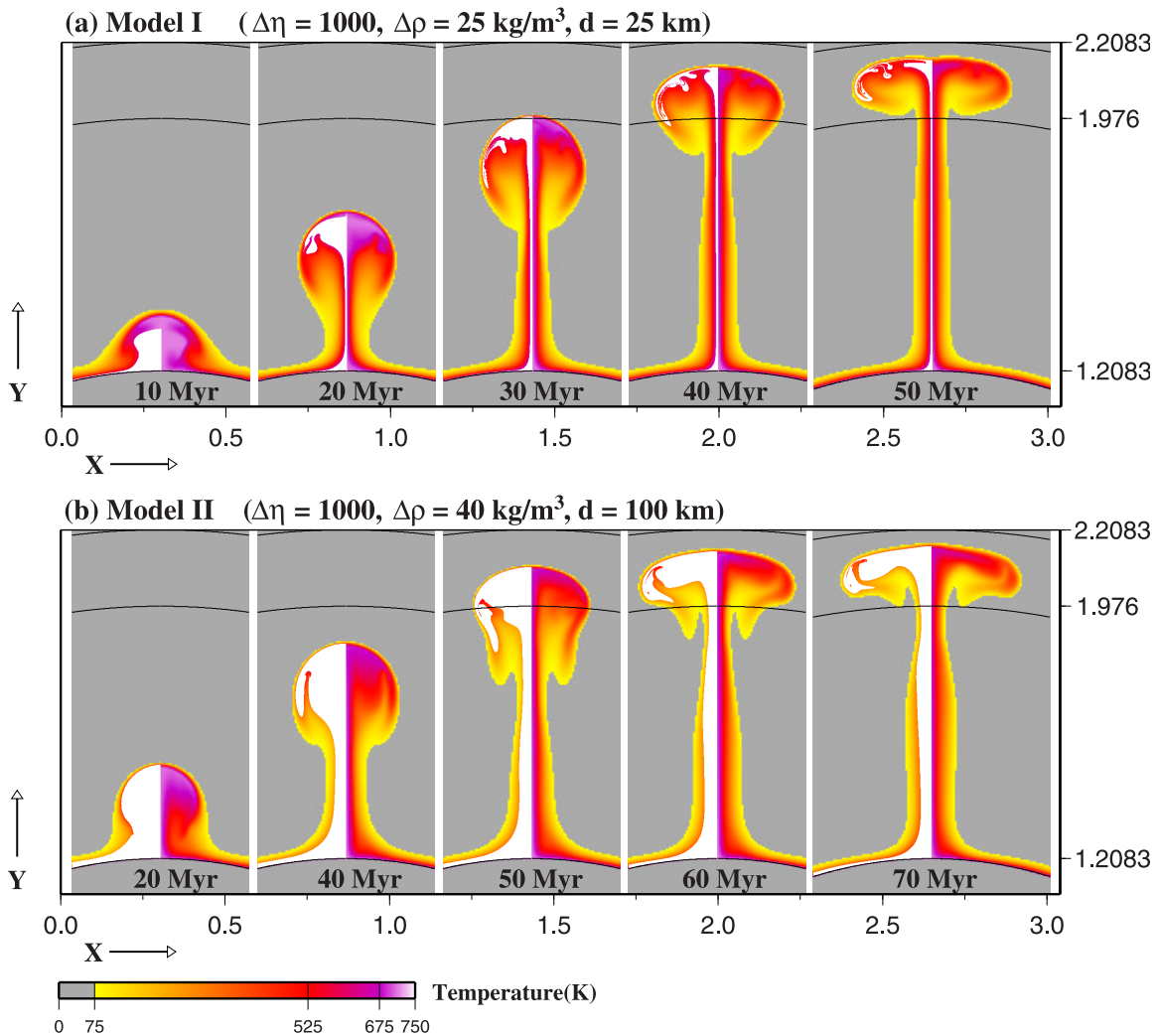

Figure 2. Examples for plumes in category I. The white color marks the distribution of the distinct composition. Length is rescaled by the thickness of the mantle (2885 km). The nondimensional values marked on the east boundaries (1.2083, 1.976, 2.2083) and the corresponding black lines at three depth levels represent CMB, 670-km discontinuity, and surface, respectively. Same notation is used throughout the paper. Model parameters: (a) Model I at five time steps: $\Delta\rho = 25$ kg/m^3, $B = 0.28$, $d = 25$ km; (b) Model II at five time steps: $\Delta\rho = 40$ kg/m^3, $B = 0.44$, $d = 100$ km.

the early stages in this model. Figure 5b and Animation 7 show that the entrainment of a thinner layer causes a much more complicated flow pattern and generate significant lateral compositional heterogeneities in the plume head ($\Delta\rho = 50$ kg/m^3, $B = 0.56$, $d = 25$ km). The entrainment of the dense material induces a counter circulation. Downward flow in the plume head and a stagnation point at the plume axis are present from 10 to 20 Myr. This leads to a lower-temperature region at the center of the plume head. The counter circulation is gradually replaced by the upwelling when the plume is established and the TBL supplies more high temperature material to the plume tail. Note that the velocity of the dense material shows significant acceleration

at depth of 670–1000 km because of the density inversion of the eclogitic material in our models.

3.2. Category II: Substantial Topography at the Base of the Plume

[13] When the thickness of the compositional layer is ~≥80 km and intrinsic density contrast is ≥60 kg/m^3, a significant volume of the dense material is sucked toward the plume and piles up at the base of the plume. It forms a large-scale undulation of the interface between the compositional layer and the overlying mantle. Various types of the plume development and entrainment of dense material associated with this large-scale undulation are observed. Figure 6 and Animation 8 show the
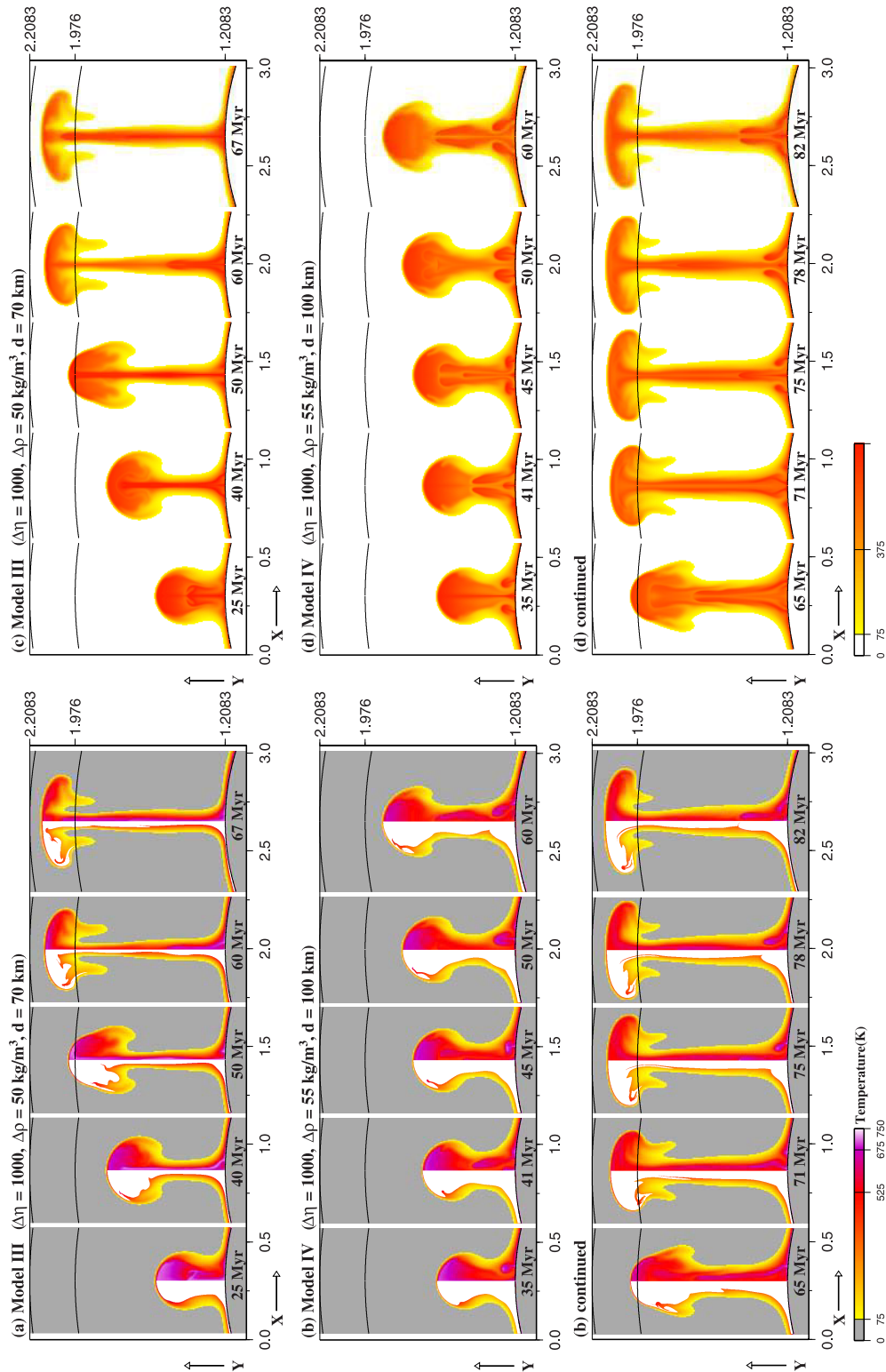
Figure 3. Examples for plumes with frequent pulsations in category I. Model parameters: (a and c) Model III at five time steps: $\Delta\rho = 50$ kg/m³, $B = 0.56$, $d = 70$ km; (b and d) Model IV at ten time steps: $\Delta\rho = 55$ kg/m³, $B = 0.61$, $d = 100$ km. Thermal field is colored by two color palettes throughout the paper to emphasize various details when a separate panel for the thermal field is necessary. Notice that the only difference between Figures 3a and 3c, or Figures 3b and 3d, is the color palette.
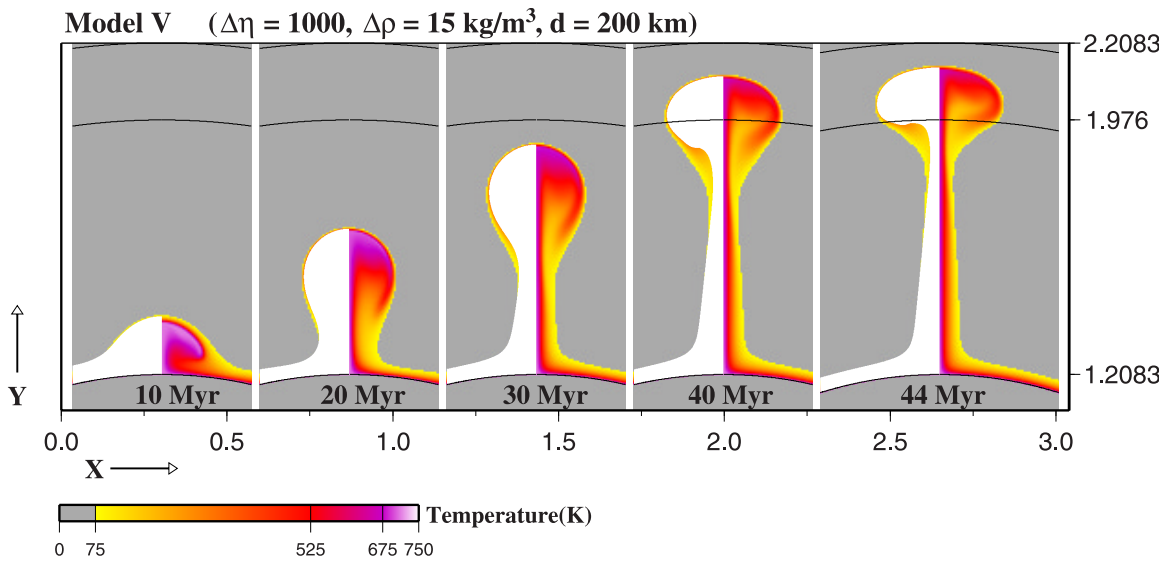
Figure 4. Example of plumes with thick dense layer in category I. Model parameters: Model V at five time steps, $\Delta\rho = 15$ kg/m^3, $B = 0.17$, $d = 200$ km.

formation of a large plume head and substantial topography at the base of the plume starting at 50 Myr ($\Delta\rho = 65$ kg/m^3, $B = 0.72$, $d = 100$ km). The compositional layer is weak due to the strongly temperature-dependent viscosity, which allows significant deformation of the TBL and strong small-scale convection at the base of the plume. The upward velocity of the plume head is significantly decreased because the compositional density reduces the positive thermal buoyancy. The temperature of plume head and plume conduit becomes lower as the plume spreads during its ascent. At ∼70 Myr, another instability of relatively small volume but with high temperature develops from the base of the plume tail. It propagates along the plume conduit and subsequently elevates the temperature of plume tail. The large-scale undulation is a persistent feature and lasts for more than 100 million years. The topography formed by the distinct composition is on the order of 1000 km and its shape is concave upward.

[14] When the thickness of the dense material increases further, the small-scale convection in the compositional layer is suppressed. This leads to a lower temperature in the TBL and consequently a plume with relatively low temperature (e.g., Figure 7a and Animation 9: $\Delta\rho = 60$ kg/m^3, $B = 0.67$, $d = 150$ km, and Figure 7b and Animation 10: $\Delta\rho = 60$ kg/m^3, $B = 0.67$, $d = 175$ km). The irregular topography of the TBL extends to several hundred kilometers above the CMB. Plumes are nearly "stagnant" for tens of million years in the lower mantle due to their nearly neutral buoyancy.

When the intrinsic density increases, the dense material initially forms a dome (e.g., Figure 8 and Animation 11: $\Delta\rho = 75$ kg/m^3, $B = 0.83$, $d = 125$ km). A cool and well-rounded thermal plume head is formed from the upper portion of TBL. This is followed by a warmer pulse with subsequent entrainment of the dense material. The topography of the compositional layer is relatively flat. A similar two-stage plume is generated with a thinner and denser layer. In this case, a larger blob of dense material is entrained (e.g., Figure 9 and Animation 12: $\Delta\rho = 75$ kg/m^3, $B = 0.83$, $d = 80$ km). The upward velocity of plume head is much higher. A downward flow develops within the ascending plume head before the plume head reaches the depth range of 670–1000 km similar to the plume shown in Figure 5. Upwellings at the base of the plume axis are suppressed and the upper portion of the TBL supplies material to the plume starting at ∼70 million years. Similar processes are also observed in some of the previous models. It shows that the plume material can be entrained from different areas of the TBL during the evolution of the plume.

3.3. Category III: Multiple Pulsations With Large Material Flux

[15] The third category of plumes is characterized by multiple, large pulsations that occur when the density and thickness of the compositional layer is in between that of models in categories I and II. Dense material accumulated around the plume axis induces secondary instabilities with large volume
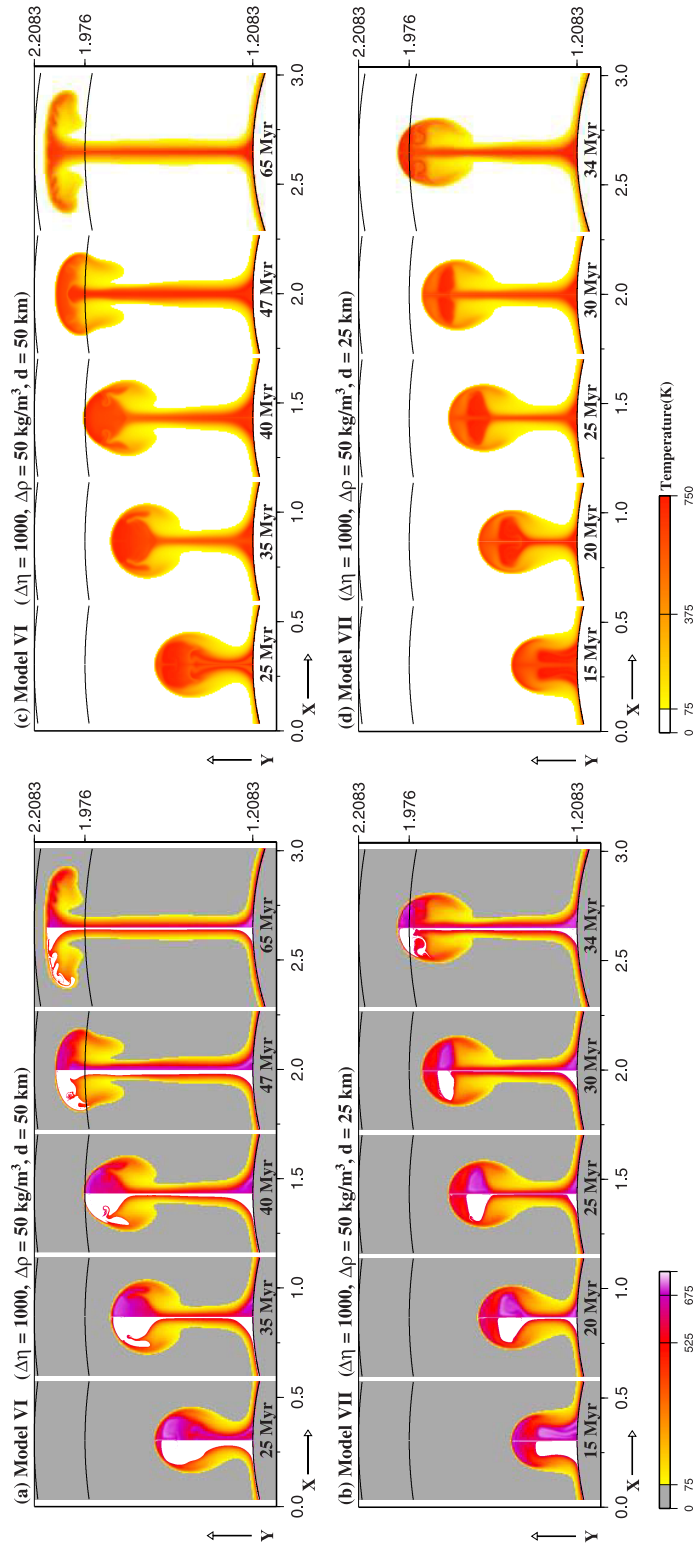
Figure 5. Example of plumes in category I with high intrinsic density contrast, and a thin dense layer. High temperature, intrinsically dense material is surrounded by lower temperature material. Model parameters: (a and c) Model VI at five time steps: $\Delta\rho = 50$ kg/m³, $B = 0.56$, $d = 50$ km; (b and d) Model VII at five time steps: $\Delta\rho = 50$ kg/ m³, $B = 0.56$, $d = 25$ km.
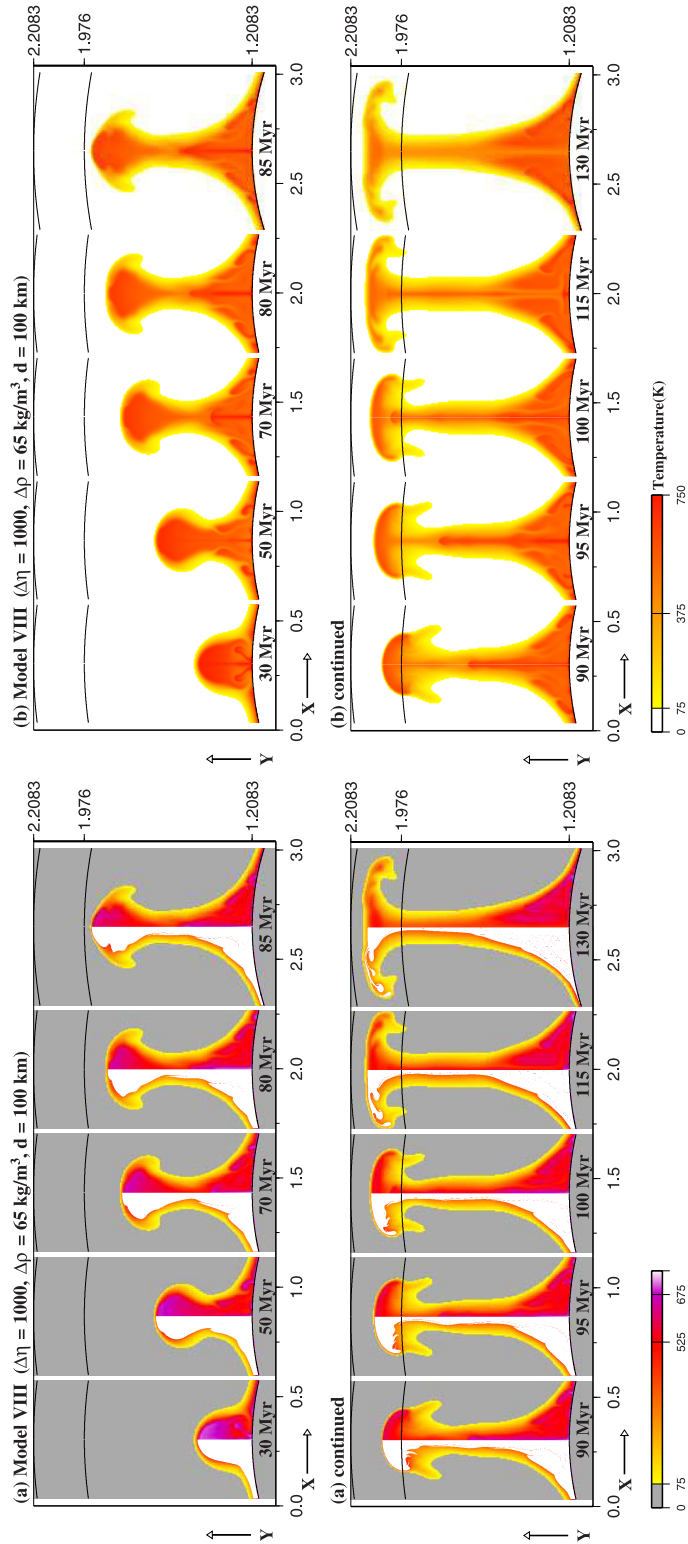
Figure 6. Example of plumes in category II. Substantial topography of the compositional layer is developed simultaneously with the formation of plume. Model parameters: Model VIII at ten time steps: $\Delta\rho = 65$ kg/m³, $B = 0.72$, $d = 100$ km.
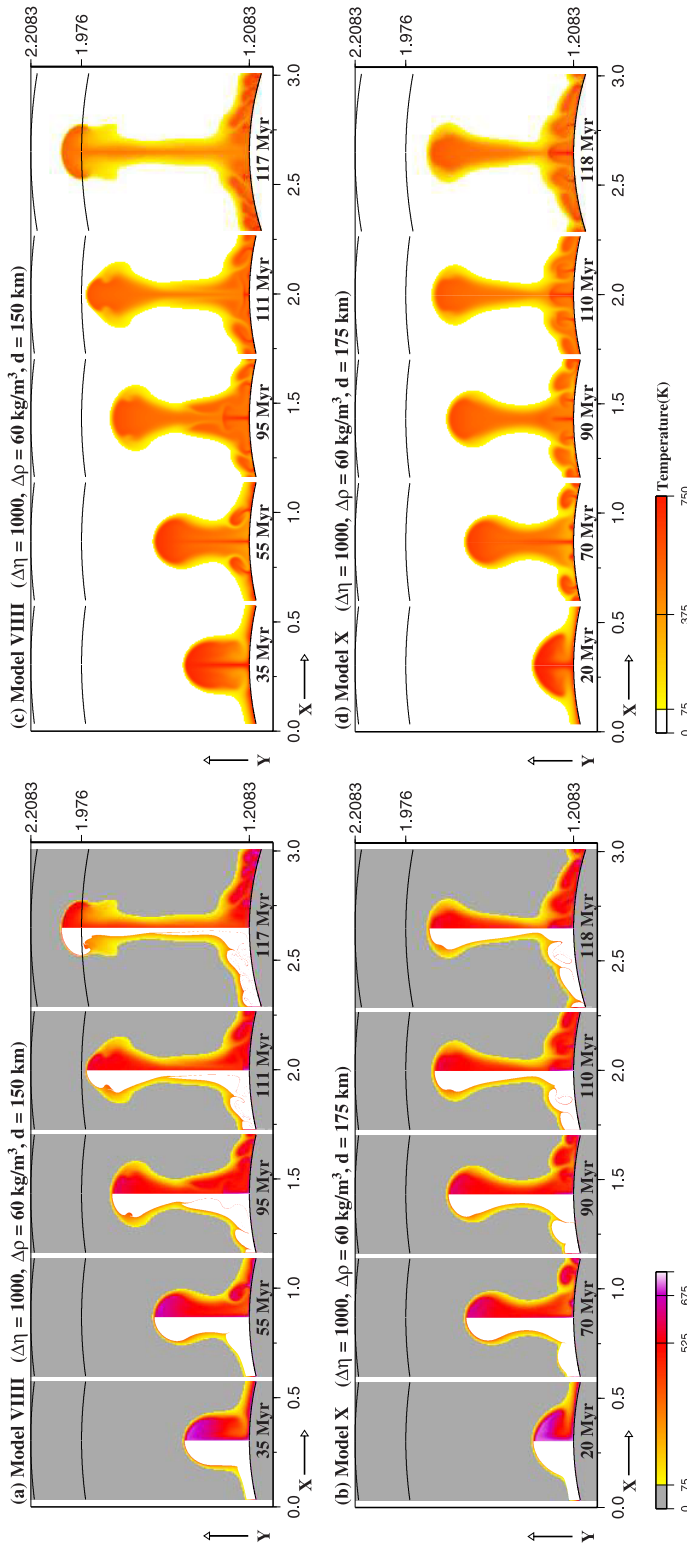
Figure 7. Examples of plumes in category II. The upward velocity of the plume head is much lower due to the nearly neutral buoyancy. The plume head stays in the lower mantle for more than 70 million years. Model parameters: (a and c) Model VIIII at five time steps: $\Delta\rho = 60$ kg/m³, $B = 0.67$, $d = 150$ km; (b and d) Model X at five time steps: $\Delta\rho = 60$ kg/m³, $B = 0.67$, $d = 175$ km.

(a) Model XI ($\Delta\eta$ = 1000, $\Delta\rho$ = 75 kg/m³, d = 125 km)

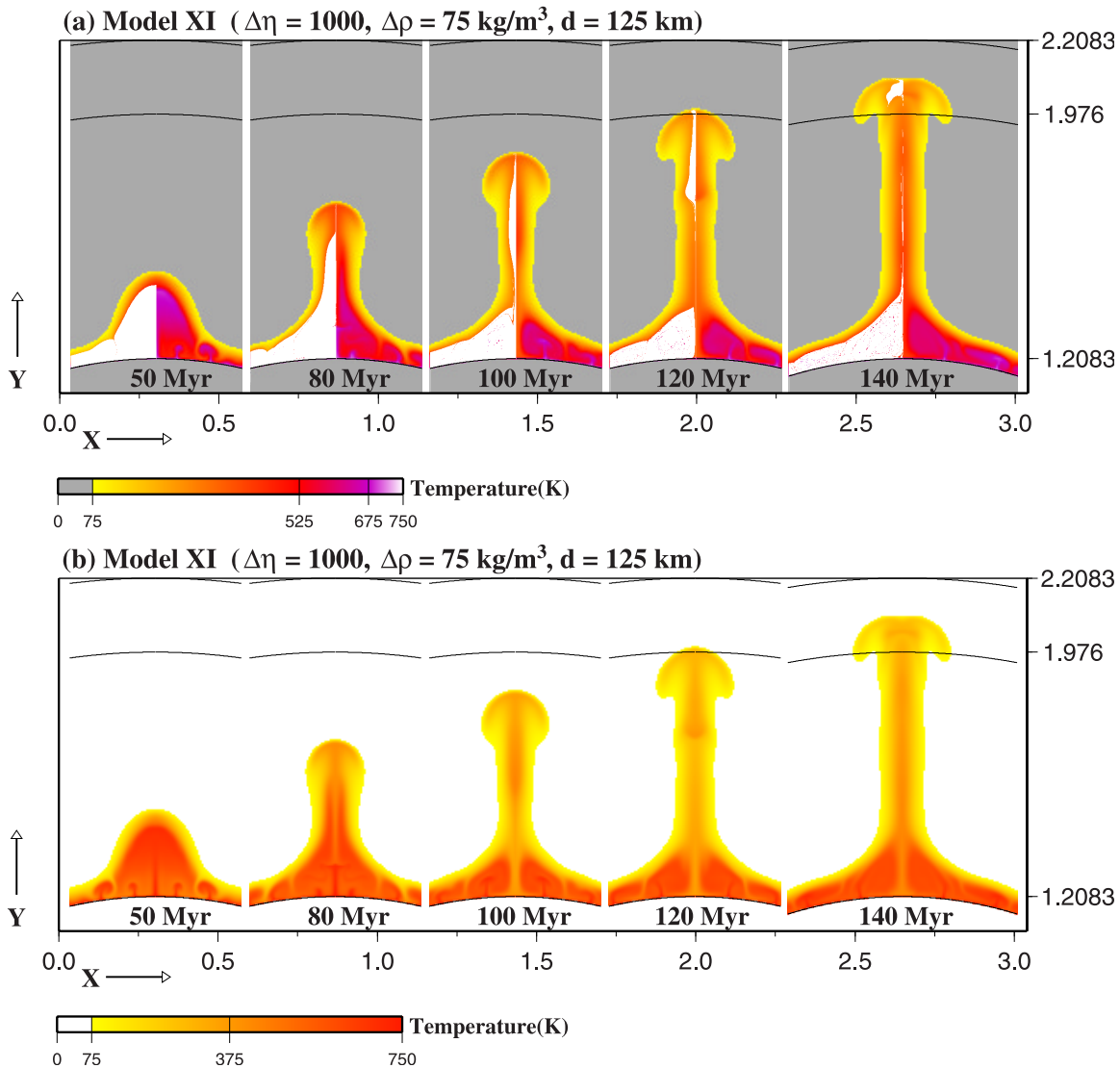**(b) Model XI ($\Delta\eta$ = 1000, $\Delta\rho$ = 75 kg/m³, d = 125 km)**

Figure 8. Example of plumes in category II with lower temperature. The dense material forms a dome at ~50 Myr. Model parameters: Model XI at five time steps: $\Delta\rho$ = 75 kg/m³, B = 0.83, d = 125 km.

and eventually migrate laterally and converge to the plume conduit when the thickness of compositional layer is ~$\geq$100 km and the intrinsic density contrast is $\geq$50 kg/m³ or if the thickness is ~$\geq$125 km and the density contrast is $\geq$40 kg/m³. This leads to subsequent pulses within the plume in which the material flux is similar to that of the primary plume head (e.g., Figure 10 and Animation 13: $\Delta\rho$ = 40 kg/m³, B = 0.44, d = 150 km, and Figure 11 and Animation 14: $\Delta\rho$ = 40 kg/m³, B = 0.44, d = 125 km). The convergence of the secondary instabilities forms a temporary large-scale undulation of the TBL. The plume conduit becomes significantly wider when the subsequent material supplement propagates along the conduit. The topography of the TBL at the base of the plume, the radius of the plume conduit and the temperature field in the plume are strongly time-dependent. Plumes can no longer be described as consisting of a single plume head with a steady conduit. The entire plume is dominated by entrained material.

3.4. Evolution of Buoyancy Flux

[16] The buoyancy flux is a measure of strength of plumes and is usually estimated by the associated surface topography [e.g., *Davies*, 1988; *Sleep*, 1990]. Figure 12 shows the temporal evolution of the nondimensional buoyancy flux (B_c) as a function of thickness and intrinsic density contrast of the distinct compositional layer for models with strongly temperature-dependent viscosity. The relative buoyancy flux here is calculated according to
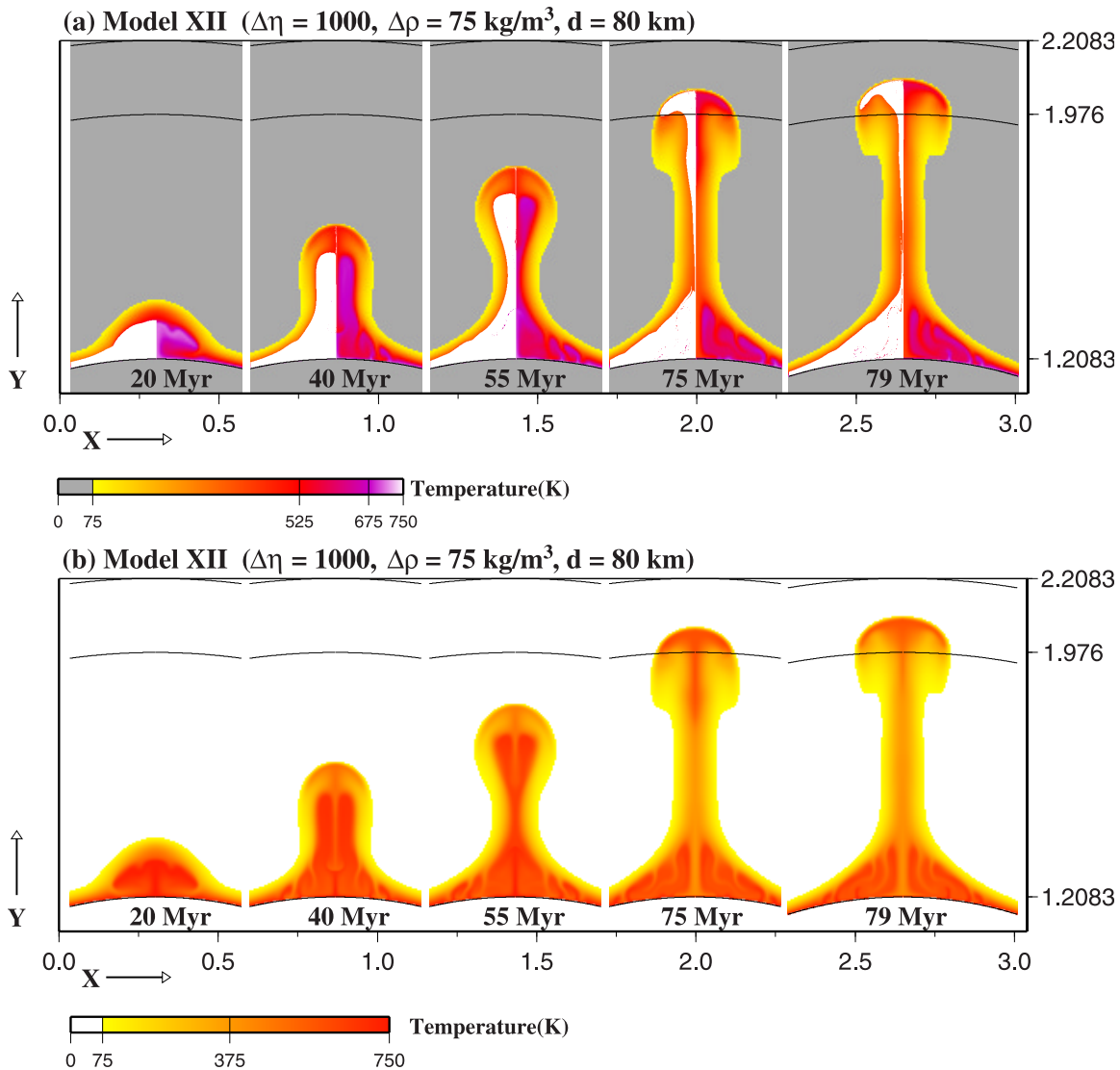
Figure 9. Example of plumes in category II. Considerable amount of dense material is sheared and entrained into the plume head. Model parameters: Model XII at five time steps: $\Delta\rho = 75$ kg/m^3, $B = 0.83$, $d = 80$ km.

equation $B_c = \int w\mathrm{T}dA/B(c, max)$ at 600-km depth, where w is the nondimensional normal velocity, T the nondimensional temperature, dA the nondimensional area and $B(c, max)$ the maximum value of the buoyancy flux in each model. As can be expected, plumes reach the upper mantle more slowly when the thickness of the compositional layer is larger or its intrinsic density contrast is higher. A great variety of the evolution for the buoyancy flux is observed. Similar behaviors for the models with moderately temperature-dependent viscosity are observed. The small amplitude variations in the buoyancy flux are caused by small-volume insta-bilities. Major secondary pulsations are caused by significant material flux for models in category III. The time gap between two major pulses ranges

from a few million to more than one hundred million years. In a few cases, the secondary pulses can be stronger than the arrival of primary plume head in strength. The pulsating plumes may con-tribute to the multiple episodes of large igneous provinces [*Lin and van Keken*, 2005].

4. Discussion and Conclusions

4.1. Diversity of Plume Structures

[17] We observe diverse behavior of the evolution of plumes in our model system. The thickness and the intrinsic density contrast both control the for-mation of plumes. The radius of the plume conduit ranges from a few tens to a few hundred of kilo-
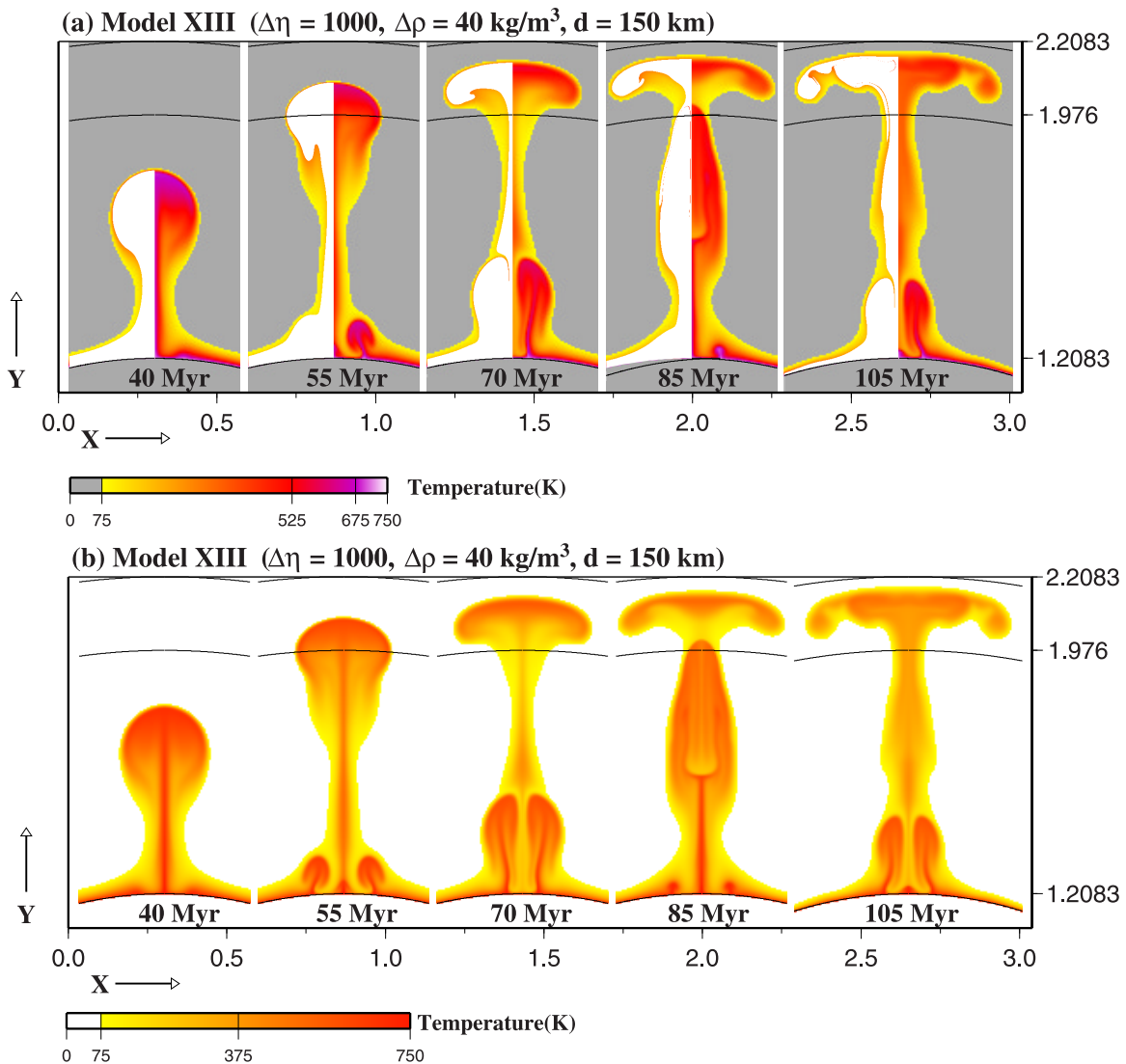
Figure 10. Example of plumes in category III. Secondary instabilities with substantial material flux replenish the plume head. Model parameters: Model XIII at five time steps: $\Delta\rho = 40$ kg/m³, $B = 0.44$, $d = 150$ km.

meters. The morphology of the plume head changes from a sphere to be stretched or elongated. Average temperature at the plume axis in the upper mantle ranges from $\sim\leq20\%$ to 90% of the maximum thermal perturbation in the TBL [*Lin and van Keken*, 2006]. In many cases, plumes can no longer be described as consisting of a single voluminous plume head followed by a steady narrow plume tail. The TBL around the base of the plume can be drained by the formation of the plume, or pile up at the base of the plume and form large-scale undulations, in which the interface between the compositional layer and the overlying mantle has variable morphology. The radius and shape of the plume conduit and the substantial topography of the compositional layer can be strongly time-depen-

dent. The internal structure of the plumes is modified by the entrainment of the dense material. In general, the dense material has the highest temperature in the plume. Plumes can ascend and reach the subsurface within several tens of million years, but can also be nearly stagnant for tens of million years in the lower mantle. Secondary instabilities play an important role in the deformation and the formation of the lateral heterogeneity in the plumes in a wide range of parameter space. The flow field in the plume head is often strongly influenced by the presence of the dense material or the material flux of secondary instabilities. The thermal field and the distribution of dense material often vary significantly along the plume axis and in the plume head. The plume head or the outer

shell of the plume conduit frequently has a higher temperature than that in the center of the plume. Strongly lateral heterogeneity in compositional and thermal fields is a common feature. The length scale of the heterogeneity can be as small as a few kilometers and the time scale can be on the order of a few millions years. These observations suggest that the corresponding seismic signatures are likely much more complicated than the classic plume structure of a large plume head versus thin plume conduit.

[18] In our calculations, plumes can consist almost entirely the entrained intrinsically dense material under a wide range of conditions. Previous laboratory experiment for purely compositional plumes show two type of structures, dependent on the viscosity ratio between plume and ambient fluid [*Kumagai*, 2002]. The first type occurs at small viscosity ratio ($\Delta \eta \leq 11$) and resembles thermal plumes with high viscosity ratio observed in some previous experiments [*Kumagai*, 2002]. The second type shows chaotic stirring in the plume head at high viscosity ratio ($104 \leq \Delta\eta \leq 856$). We do not observe similar structures. In our models, the stirring in the plume head is mainly determined by the secondary instabilities when the entire plume is basically composed by the material from the compositional layer. The effects of thermal buoyancy in our models combined with the different rheologies and mechanisms of the material supply between the numerical and analogue experiments likely cause the differences. Moreover, the axisymmetric condition in our experiments forces the convection to two-dimension and may suppress the nonlinearity in the system. This may result in the less chaotic behavior in our models.

4.2. Large-Scale Undulation of the Compositional Layer

[19] The compositional layer can be deformed actively by the small-scale convection when the compositional layer piles up beneath the base of the plume tail. Substantial topography of the compositional layer is developed in the lower mantle. Both the intrinsic density contrast and the thickness of the compositional layer influence the shape of the interface between the compositional layer and the overlying mantle. Small-scale convection in the TBL may contribute to the lateral heterogeneities observed in the D'' layer. The length-scale of the strongly lateral heterogeneity of the temperature field can be on the order of 100 km. The substantial topography is a persistent feature over the geolog-

ical time. Under certain conditions plumes are almost stagnant in the lower mantle for tens of million years.

[20] Two broad low seismic velocity regions beneath south central Pacific and beneath the southern Atlantic Ocean and Africa are correlated to the major geoid highs and to the concentration of hot spots [e.g., *Hager et al.*, 1985; *Su et al.*, 1994; *Schubert et al.*, 2004]. The low seismic velocity signatures continuously extend from the base of the mantle to several hundred kilometers above core-mantle boundary to even the base of the lithosphere. These features may be related to the presence of a compositional layer in the lowermost mantle [e.g., *Su et al.*, 1994; *Ritsema et al.*, 1999; *Romanowicz and Gung*, 2002; *Ni and Helmberger*, 2003]. They have been considered as broad mantle upwelling, superplumes, piles, or plume clusters [e.g., *Forte and Mitrovica*, 2001; *Davaille*, 1999; *Davaille et al.*, 2002; *Tackley*, 1998; *Jellinek and Manga*, 2004; *McNamara and Zhong*, 2004; *Schubert et al.*, 2004]. The features observed in our models, including the large-scale undulation of the interface between the compositional layer and the overlying mantle, the simultaneous development of plume with the undulation and the temporarily stagnant plume in the lower mantle, may contribute to the formation of these two large low velocity provinces.

4.3. Surface Topography Swell

[21] The uplifted topography associated with intraplate volcanism has been used to estimate the buoyancy flux of mantle plumes and as a criterion for mapping the mantle plumes [e.g., *Davies*, 1988; *Sleep*, 1990]. It has been argued that some oceanic plateaux such as Ontong Java were not caused by a mantle plume because the high elevated surface topography and expected subsidence rate that should be associated with the high temperature material in the upper mantle is not observed [e.g., *Ingle and Coffin*, 2004]. Our model results show that mantle plumes may consist of large amounts of hot but compositionally dense material. The presence of the dense material would reduce the net buoyancy force within the thermochemical plumes with subsequent reduction of topographic effects. It suggests that the use of excess topography may not always provide an appropriate criterion for mapping mantle plumes. In addition, the reduction in swell topography will cause an underestimate of the core-mantle boundary heat flux in the approach of *Davies* [1988] and *Sleep* [1990]. This suggests that the core mantle boundary heat flux could be

(a) Model XIV ($\Delta\eta = 1000$, $\Delta\rho = 40$ kg/m^3, d = 125 km)

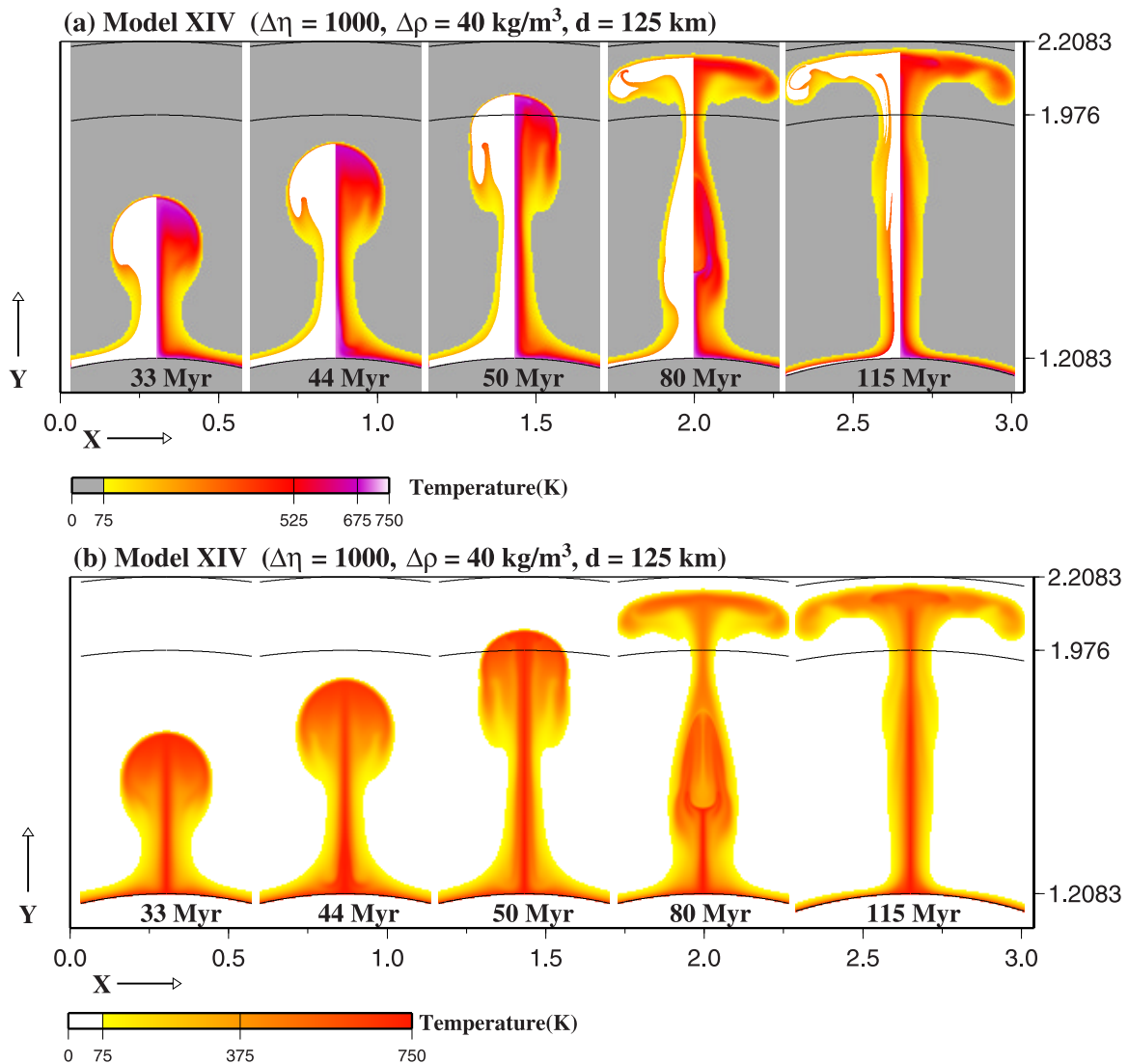**(b) Model XIV ($\Delta\eta = 1000$, $\Delta\rho = 40$ kg/m^3, d = 125 km)**

Figure 11. Example of plumes in category III. The shape of the plume head is enlarged at ~50 Myr and secondary instabilities develop and replenish the plume head subsequently. Model parameters: Model XIV at five time steps, $\Delta\rho = 40$ kg/m^3, $B = 0.44$, $d = 125$ km.

potentially significantly higher than previously estimated.

4.4. Sensitivity of Model Parameters and Model Applicability to the Earth's Mantle

[22] Our result shows that the structures of the thermochemical plumes can be complicated even under the relatively simple assumptions for the initial conditions used in our models. We expect that the dense basal layer may show undulations and internal heterogeneity. This would result in regional differences in the type of plumes that can be generated.

[23] The amount of entrainment predicted in our models provides some constraints on the properties of the dense layer since low density contrasts would lead to rapid entrainment and erosion of the dense layer. This effect is mitigated if our assumption that the dense layer is maintained by subduction of eclogite is correct. We can make a zeroth order approximation to the rate of erosion by assuming that plumes in the lower mantle have a typical radius of 100 km, an entrainment rate of the dense layer of 10% and an upward velocity of 5 cm/yr. If we further assume that we have 10 such plumes we find an volumetric erosion rate of 12 km^3/yr, which can be compared to the oceanic crust production (and assumed recycling rate) of 18 km^3/yr. The near balance suggests that we can actively maintain such a dense layer under these assumptions.
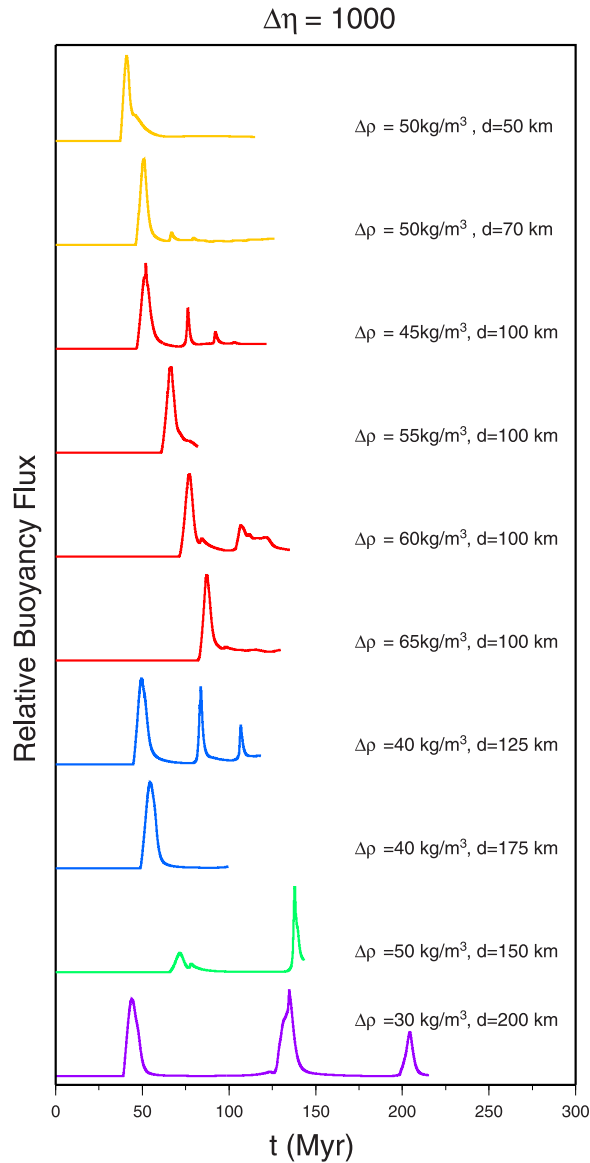
Δη = 1000

Δρ = 50kg/m³ , d=50 km

Δρ = 50kg/m³ , d=70 km

Δρ = 45kg/m³, d=100 km

Δρ = 55kg/m³, d=100 km

Δρ = 60kg/m³, d=100 km

Δρ = 65kg/m³, d=100 km

Δρ =40 kg/m³, d=125 km

Δρ =40 kg/m³, d=175 km

Δρ =50 kg/m³, d=150 km

Δρ =30 kg/m³, d=200 km

Relative Buoyancy Flux

t (Myr)

Figure 12. Temporal evolution of nondimensional buoyancy flux for selected models with strongly temperature-dependent viscosity (Δη = 1000). The vertical axis shows the amplitude of plume flux normalized by the maximum value for each model.

[24] The strategy we adopted for this study is to allow for the exploration of the plume structure in a thermochemical convection system that covers plausible range of physical parameters in a systematic manner. Several factors should be considered when apply our model results to Earth's mantle. Our calculations are sensitive to the initial condition. We initiate plumes from a small thermal perturbation that can be thought of as a bump on the TBL that naturally develop in the actively convecting mantle. We assumed a thickness of 130 km

for the TBL and a specific thermal buoyancy contrast. Clearly, these are expected to vary across the lowermost mantle. To an extent we can generalize the conclusions by considering the nondimensional density ratio (between thermal and compositional buoyancy) and the nondimensional thickness (between that of the TBL and the dense layer).

[25] We ignore convection driven by the subduction of plates which may be reasonable if the small scale plume flow can indeed be decoupled from the large scale flow. This decoupling is enhanced by the strong temperature-dependence of rheology and the overall sluggishness of mantle convection expected for a high viscosity lower mantle, but it is likely that the type of plume behavior we predict will only occur away from zones of active or paleo subduction.

Appendix A: Entrainment—A Comparison With Scaling Theories

[26] The entrainment for flow driven by plumes is estimated by *Sleep* [1988]. It can be approximately described as

$$F = C_0/B^2 \qquad (A1)$$

where C_0 is a constant. Figure A1a shows volume fraction of the entrained dense material as a function of buoyancy number. The solid line is equation (A1) with $C_0 = 0.07$. The numerical experiments with various thickness are consistent with the scaling relationship. The entrainment is more profound in the models with lower buoyancy number as shown in previous studies [e. g., *Sleep*, 1988; *Davaille*, 1999; *Davaille et al.*, 2002; *Zhong and Hager*, 2003; *McNamara and Zhong*, 2004].

[27] *Davaille* [1999] derived the scaling relationship for volumetric flux of entrained material across the interface based on the balance between buoyancy forces and viscous forces:

$$Q = C_1 \kappa H B^{-2} Ra^{1/3} \frac{1}{1 + \Delta\eta/B} \qquad (A2)$$

where C_1 is an experiment constant. Our results agree well with equation (A2) with $C_1 = 1.1$ when $B \sim \leq 1$ but are significantly smaller if $B \sim \geq 1$ even for a thin dense layer (e.g., 25 km) (Figure A1b). The difference may result from that we use constant values of B and Rayleigh number to calculate the value of Q, while the effective B and thermal Rayleigh number for entrainment would vary with time and the properties of the dense layer. For example, in the case with a thin dense layer with
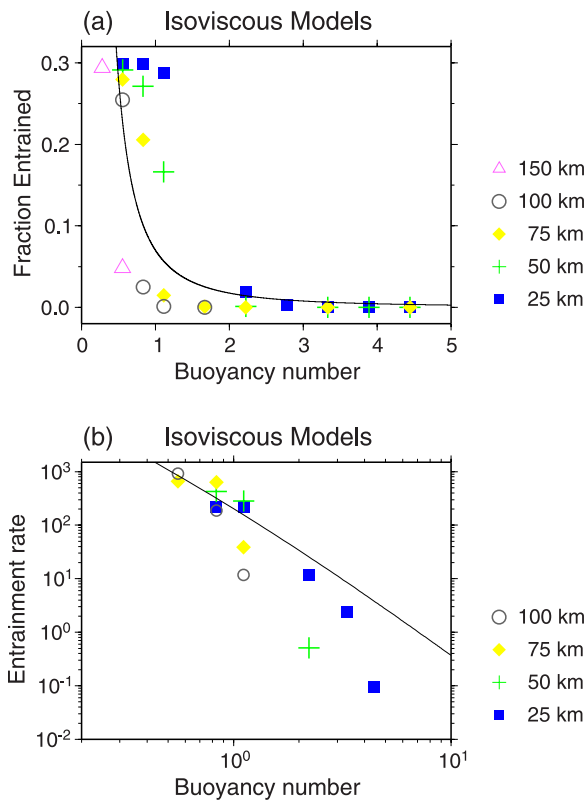
Figure A1. (a) Volume fraction of entrained dense material as a function of buoyancy number. The entrained fraction is calculated on the basis of the volume of the entrained material in the upper mantle at snapshot of 300 Myr. Symbols with various colors mark the fraction for models with different initial thickness. The solid line is equation (A1) with $C_0 = 0.07$. (b) Volumetric entrainment rate (Q, m^3/s) of dense material as a function of buoyancy number. The value of Q is calculated roughly on the basis of the result right before the development of secondary instability in the region other than the initial thermal perturbation near the plume axis. The solid line stands for equation (A2) with $C_1 = 1.1$.

high chemical density contrast, the dense material prevents the lowermost portion of the thermal boundary layer to become involved with plume formation [e.g., *Lin and van Keken*, 2006]. This process would reduce the plume temperature and effective Rayleigh number and increase the value of B. The predicted Q value would further approach to our model results for models with B ≥ 1 when this effect is considered.

[28] The comparison between these relationships and our models with temperature-dependent viscosity is much more difficult because the entrainment of these models are commonly strongly time-dependent [*Lin and van Keken*, 2006] and our calculations only consider relatively short time

period (several hundred million years). Representative values for comparison such as a constant entrainment rate or average value based on complete erosion of the dense layer cannot be obtained.

References

Anderson, D. L. (1998), The EDGES of the mantle, in *The Core-Mantle Boundary Region*, *Geodyn. Ser.*, vol. 28, edited by Gurnis, M., et al., pp. 255–271, AGU, Washington, D. C.

Anderson, D. L. (2004), Scoring hotspots: The plume and plate paradigms, in *Plates, Plumes and Paradigms*, edited by Foulger, G. R. et al., *Spec. Pap. Geol. Soc. Am.*, 388.

Boehler, R. (2000), High pressure experiments and the phase digram of lower mantle and core materials, *Rev. Geophys.*, 38, 221–245.

Christensen, U. R., and A. W. Hofmann (1994), Segregation of subducted oceanic crust in the convecting mantle, *J. Geophys. Res.*, 99, 19,867–19,884.

Condie, K. C. (2001), *Mantle Plumes and Their Record in Earth History*, Cambridge Univ. Press, New York.

Courtillot, V., A. Davaille, J. Besse, and J. Stock (2003), Three distinct types of hotspots in the Earth's mantle, *Earth Planet. Sci. Lett.*, 205, 295–308.

Cuvelier, C., A. Segal, and A. van Steenhoven (1986), *Finite Element Methods and the Navier-Stokes equations*, Springer, New York.

Davaille, A. (1999), Simultaneous generation of hotspots and superswells by convection in a heterogeneous planetary mantle, *Nature*, 402, 756–760.

Davaille, A., F. Girard, and M. Le Bars (2002), How to anchor hotspots in convective mantle?, *Earth Planet. Sci. Lett.*, 203, 621–623.

Davies, G. F. (1988), Ocean bathymetry and mantle convection: 1. Large-scale flow and hotspots, *J. Geophys. Res.*, 93, 10,467–10,480.

Davies, G. F. M. (1999), *Dynamic Earth: Plates, Plumes and Mantle Convection*, Cambridge Univ. Press, New York.

Ebinger, C. J., and N. H. Sleep (1998), Cenozoic magmatism throughout east Africa resulting from impact of a single plume, *Nature*, 395, 788–791.

Farnetani, C. G., and H. Samuel (2005), Beyond the thermal plume paradigm, *Geophys. Res. Lett.*, 32, L07311, doi:10.1029/2005GL022360.

Forte, A. M., and J. X. Mitrovica (2001), Deep-mantle high-viscosity flow and thermochemical structures inferred from seismic and geodynamic data, *Nature*, 410, 1049–1056.

Foulger, G. R., and J. H. Natland (2003), Is "hotspot" volcanism a consequence of plate tectonics?, *Science*, 300, 921–922.

Goes, S., F. Cammarano, and U. Hansen (2004), Synthetic seismic signature of thermal mantle plumes, *Earth Planet. Sci. Lett.*, 218, 403–419.

Grand, S. P., R. D. van der Hilst, and S. Widiyantoro (1997), Global seismic tomography: A snapshot of convection in the Earth, *GSA Today*, 7, 107.

Griffiths, R. W., and I. H. Campbell (1990), Stirring and structure in mantle plumes, *Earth Planet. Sci. Lett.*, 99, 66–78.

Gu, Y. J., A. M. Dziewonski, W. Su, and G. Ekstrom (2001), Models of the mantle shear velocity and discontinuities in the pattern of lateral heterogeneities, *J. Geophys. Res.*, *106*, 11,169–11,199.

Hager, B. H., R. W. Clayton, M. A. Richards, R. P. Corner, and A. M. Dziewonski (1985), Lower mantle heterogeneity, dynamic topography and the geoid, *Nature*, *313*, 541–545.

Ingle, S., and M. F. Coffin (2004), Impact origin for the greater Ontong Java Plateau?, *Earth Planet. Sci. Lett.*, *218*, 123–134.

Jeanloz, R., and S. Morris (1986), Temperature distribution in the crust and in the mantle, *Annu. Rev. Earth Planet. Sci.*, *14*, 377–415.

Jellinek, A. M., and M. Manga (2004), Links between long-lived hot spots, mantle plumes, D′, and plate tectonics, *Rev. Geophys.*, *42*, RG3002, doi:10.1029/2003RG000144.

Kellogg, L. H., and S. D. King (1997), The effect of temperature dependent viscosity on the structure of new plumes in the mantle: Results of a finite element model in a spherical axisymmetrical shell, *Earth Planet. Sci. Lett.*, *148*, 13–26.

Kellogg, L. H., B. H. Hager, and R. D. van der Hilst (1999), Compositional stratification in the deep mantle, *Science*, *283*, 1881–1884.

Kumagai, I. (2002), On the anatomy of mantle plumes: Effect of the viscosity ratio on entrainment and stirring, *Earth and Planet. Sci. Lett.*, *198*, 211–224.

Lay, T., and E. J. Garnero (2004), Core-mantle boundary structures and processes, in *The State of the Planet: Frontiers and Challenges in Geophysics*, *Geophys. Monogr. Ser.*, vol. 150, edited by R. S. J. Spark and C. J. Hawkesworth, pp. 25–41, AGU, Washington, D. C.

Lin, S. C., and P. E. van Keken (2005), Multiple volcanic episodes of flood basalts caused by thermochemical mantle plumes, *Nature*, *436*, doi:10.1038/nature03697, 250–252.

Lin, S.-C., and P. E. van Keken (2006), Dynamics of thermochemical plumes: 1. Plume formation and entrainment of a dense layer, *Geochem. Geophys. Geosyst.*, *7*, Q02006, doi:10.1029/2005GC001071.

Lin, S. C., B. Y. Kuo, L. Y. Chiao, and P. E. van Keken (2005), Thermal plume models and melt generation in East Africa: A dynamic modeling approach, *Earth Planet. Sci. Lett.*, *237*, 175–192.

Loper, D., and T. Lay (1995), The core-mantle boundary region, *J. Geophys. Res.*, *100*, 6379–6420.

Manga, M., and R. Jeanloz (1996), Implications of a metal-bearing chemical boundary layer in D″ for mantle dynamics, *Geophys. Res. Lett.*, *23*, 3091–3094.

McNamara, A. K., and S. Zhong (2004), Thermochemical structures within a spherical mantle: Superplumes or piles?, *J. Geophys. Res.*, *109*, B07402, doi:10.1029/2003JB002847.

Montelli, R., G. Nolet, F. A. Dahlen, G. Maters, and E. R. Engdahl (2004), Finite-frequency tomography reveals a variety of plumes in the mantle, *Science*, *303*, 338–343.

Morgan, W. J. (1971), Convection plumes in the lower mantle, *Nature*, *230*, 42–43.

Ni, S., and D. V. Helmberger (2003), Ridge-like lower mantle structure beneath South Africa, *J. Geophys. Res.*, *108*(B2), 2094, doi:10.1029/2001JB001545.

Olson, P., and H. Singer (1985), Creeping plumes, *J. Fluid Mech*, *158*, 511–531.

Ono, S., E. Ito, and T. Katsura (2001), Mineralogy of sub-ducted basaltic crust (MORB) from 25 to 37 GPa, and chemical heterogeneity of the lower mantle, *Earth Planet. Sci. Lett.*, *190*, 57–63.

Richards, M. A., R. A. Duncan, and V. Courtillot (1989), Flood basalt and hotspot tracks: Plume heads and tails, *Science*, *246*, 103–107.

Ritsema, J., and R. M. Allen (2003), The elusive mantle plume, *Earth Planet. Sci. Lett.*, *207*, 1–12.

Ritsema, J., H. J. van Heijst, and J. H. Woodhouse (1999), Complex shear wave velocity structure imaged beneath Africa and Iceland, *Science*, *286*, 1925–1928.

Romanowicz, B., and Y. Gung (2002), Superplumes from the core-mantle boundary to the lithosphere: Implications for heat flux, *Science*, *296*, 513–516.

Rost, S., E. J. Garnero, Q. Williams, and M. Manga (2005), Seismological constraints on a possible plume root at the core-mantle boundary, *Nature*, *435*, 666–669.

Schubert, G., G. Masters, P. Olson, and P. Tackley (2004), Superplumes or plume clusters?, *Phys. Earth Planet. Inter.*, *146*, 147–162.

Shen, Y., S. C. Solomon, I. T. Bjarnason, and C. J. Wolfe (1998), Seismic evidence for a lower-mantle origin of the Iceland Plume, *Nature*, *395*, 62–65.

Sleep, N. H. (1988), Gradual entrainment of a chemical layer at the base of the mantle by overlying convection, *Geophys. J.*, *95*, 437–447.

Sleep, N. H. (1990), Hotspots and mantle plumes: Some phenomenology, *J. Geophys. Res.*, *95*, 6715–6736.

Steinle-Neumann, G., L. Stixrude, R. E. Cohen, and O. Gülseren (2001), Elasticity of iron at the temperature of the Earth's inner core, *Nature*, *413*, 57–60.

Su, W., R. L. Woodward, and A. M. Dziewonski (1994), Degree 12 model of shear velocity heterogeneity in the mantle, *J. Geophys. Res.*, *99*, 6945–6980.

Tackley, P. J. (1998), Three-dimensional simulations of mantle convection with a thermochemical CMB boundary layer: D″?, in *The Core-Mantle Boundary Region*, *Geodyn. Ser.*, vol. 28, edited by Gurnis, M. et al., pp. 231–253, AGU, Washington, D. C.

Tackley, P. J. (2002), Strong heterogeneity caused by deep mantle layering, *Geochem. Geophys. Geosyst.*, *3*(4), 1024, doi:10.1029/2001GC000167.

Tan, E., M. Gurnis, and L. Han (2002), Slabs in the lower mantle and their modulation of plume formation, *Geochem. Geophys. Geosyst.*, *3*(11), 1067, doi:10.1029/2001GC000238.

van der Hilst, R. D. (2004), Changing views on Earth's deep mantle, *Science*, *306*, 817–818.

van der Hilst, R. D., S. Widiyantoro, and E. R. Engdahl (1997), Evidence for deep mantle circulation from global tomography, *Nature*, *386*, 578–584.

van Keken, P. E. (1997), Evolution of starting mantle plumes: A comparison between numerical and laboratory models, *Earth Planet. Sci. Lett.*, *148*, 1–11.

van Keken, P. E., and C. J. Ballentine (1999), Dynamical models of mantle volatile evolution and the role of phase transitions and temperature-dependent rheology, *J. Geophys. Res.*, *104*, 7137–7168.

van Keken, P. E., S. Karato, and D. A. Yuen (1996), Rheological control of oceanic separation in the transition zone, *Geophys. Res. Lett.*, *23*, 1821–1824.

Whitehead, J. A., and D. S. Luther (1975), Dynamics of laboratory diapir and plume models, *J. Geophys. Res.*, *80*, 705–717.

William, Q., and E. J. Garnero (1996), Seismic evidence for partial melting at the base of the Earth's mantle, *Science*, *273*, 1528–1530.

Wolfe, C. J., I. T. Bjarnason, J. C. VanDecar, and S. C. Solomon (1997), Seismic structure of the Iceland mantle plume, *Nature*, *385*, 245–247.

Zhong, S., and B. H. Hager (2003), Entrainment of a dense layer by thermal plumes, *Geophys. J. Int.*, *154*, 666–676.